

# The Morphology of Decimetric Emission from Solar Flares: GMRT Observations

M. R. Kundu and S. M. White

*Astronomy Department, University of Maryland, College Park, MD 20742*

V. I. Garaimov

*Astronomy Department, University of Maryland, College Park, MD 20742 &*

*Special Astrophysical Observatory, St. Petersburg Branch, Russian Academy of Sciences, St. Petersburg, 196140 Russia*

P. Subramanian

*Inter-University Centre for Astronomy and Astrophysics, P.O. Bag 4, Ganeshkhind, Pune-411007, India*

S. Ananthkrishnan

*National Centre for Radio Astrophysics, TIFR, P. O. Bag 3, Ganeshkhind, Pune-411007, India*

P. Janardhan

*Physical Research Laboratory, Astronomy & Astrophysics Division, Navrang-pura, Ahmedabad-380009, India*

January 26, 2006

**Abstract.** Observations of a solar flare at 617 MHz with the Giant Meter-wave Radio Telescope are used to study the morphology of flare radio emission at decimetric wavelengths. There has been very little imaging in the 500 – 1000 MHz frequency range, but it is of great interest since it corresponds to densities at which energy is believed to be released in solar flares. This event has a very distinctive morphology at 617 MHz: the radio emission is clearly resolved by the 30'' beam into arc-shaped sources seeming to lie at the tops of long loops, anchored at one end in the active region in which the flare occurs, with the other end lying some 200000 km away in a region of quiet solar atmosphere. Microwave images show fairly conventional behaviour for the flare in the active region: it consists of two compact sources overlying regions of opposite magnetic polarity in the photosphere. The decimetric emission is confined to the period leading up to the impulsive phase of the flare, and does not extend over a wide frequency range. This fact suggests a flare mechanism in which the magnetic field at considerable height in the corona is destabilized a few minutes prior to the main energy release lower in the corona. The radio morphology also suggests that the radiating electrons are trapped near the tops of magnetic loops, and therefore may have pitch angles near 90°.

**Keywords:** Sun: flares – Sun: corona – Sun: radio radiation

## 1. Introduction

There has been essentially no imaging of solar radio bursts in the decimetric wavelength range (frequencies 500 to 1000 MHz), although there has been extensive monitoring of fluxes in this range, notably by the ETH-Zurich radio group (Güdel and Benz, 1988; Isliker and Benz, 1994; Benz, 2004) and the Ondrejov group (Jiříčka et al., 2001; Jiříčka et al., 2002). From this monitoring it is known that there is a wide array of (usually flare-related) bursts with distinctive morphologies in the frequency-time domain. These bursts have to be bright in order to be detected, and their behaviour is quite different from the synchrotron emission produced by accelerated electrons at higher microwave frequencies. It is therefore believed that most of these bursts are due to coherent plasma emission, or in some cases due to coherent cyclotron maser processes, with very high brightness temperatures (Dulk and Winglee, 1987; Melrose, 1999). The only true imaging observations in this range are those at 843 MHz from the Molonglo Synthesis Telescope (Gray et al., 1990), which is a one-dimensional array that used earth-rotation synthesis to achieve images with a resolution of 43'' × 110''. The Nançay Radio Heliograph (NRH) makes images at the longer decimetric wavelengths (frequencies 327, 410 and 432 MHz), and the Very Large Array can make high-resolution images at 327 MHz.



Based on the characteristic properties of the solar atmosphere, at these frequencies (a plasma frequency of 500 MHz corresponds to an electron density of  $3 \times 10^9 \text{ cm}^{-3}$ ) the radio emission originates above the dense loops low in the solar atmosphere that are visible in soft X-ray and EUV images. Decimetric emission illuminates magnetic field lines that can be difficult to see at other wavelengths, and it requires energetic electrons, so the morphology of the emission is of interest because it reflects the physical location of the radiating electrons and may therefore provide clues to their genesis. Type-III-like emissions, which drift rapidly from high to low frequencies, are expected to lie on open field lines, while continua confined to a narrower frequency range are expected to be on closed field lines.

Determining the morphology of solar decimetric radio emission requires high resolution imaging observations, which can be achieved with the Giant Metre-wave Radio Telescope (GMRT) thanks to the wide range of spatial scales it samples. At 617 MHz solar maps with GMRT are likely to be quite different from both lower and higher frequencies. This frequency is usually above the range of solar noise storms which often dominate the non-flaring Sun at, e.g., 327 MHz where the Very Large Array and the Nançay Radio Heliograph (NRH) can observe, so quiet-Sun maps will be more sensitive, while flares are known to exhibit a wide range of plasma phenomena at this frequency. It is close to the plasma frequency at the level believed to separate open and closed field lines above active regions, and thus we expect to see the sources of energetic electrons which propagate from this frequency towards lower frequencies on open field lines. Observations of a solar flare on Nov. 17, 2001, at 1000 MHz using GMRT have been published by Subramanian et al. (2003) and Kundu et al. (2004), while Mercier et al. (2005) discuss the combination of higher-resolution GMRT visibilities with shorter-spacing NRH data. In this paper we report on an event observed with GMRT at 617 MHz on 2002 October 6. We compare decimetric images with microwave images of the same event from the Nobeyama Radioheliograph (NoRH) that reveal the nature of activity much lower in the corona. In this event the activity at 617 MHz precedes the main impulsive flare phase seen at other wavelengths, but it is well resolved spatially by the GMRT observations and the images reveal very interesting properties of the decimetric emission.

## 2. Observations

### 2.1. CONTEXT

Figure 1 shows the active region and surroundings in a  $195 \text{ \AA}$  Fe XII EUV image from the Extreme-ultraviolet Imaging Telescope (EIT) on the SOHO satellite at 04:36 UT, together with longitudinal magnetic field contours showing the location of sunspots within the active region. The active region is dominated by a positive-polarity leading spot, but just to the west of this spot is an arc of magnetic field of mixed polarity. At the trailing end of the active region is a negative-polarity spot and some brighter EUV emission over weaker fields. A sequence of magnetograms from SOHO/MDI shows the large spot to be rotating clockwise around the time of the event, and magnetic flux of both polarities being expelled radially outwards from the vicinity of this spot. The high-frequency radio emission from this event involves the largest spot and the trailing portion of the region. However, the decimetric emission also involves (in projection) the region in the bottom left quadrant of Fig. 1 where neither magnetic field nor pre-existing bright EUV loops are present. There were no Transition Region And Coronal Explorer (TRACE) or EIT images at EUV wavelengths of the region during the flare, and the hard X-ray telescope Reuven Ramaty High Energy Solar Spectroscopic Imager (RHESSI) was in night.

Light curves at selected radio frequencies and in soft X-rays are shown in Figure 2. In soft X-rays this was quite a short event with a rapid decline (which is why there was no sign of flare loops in the

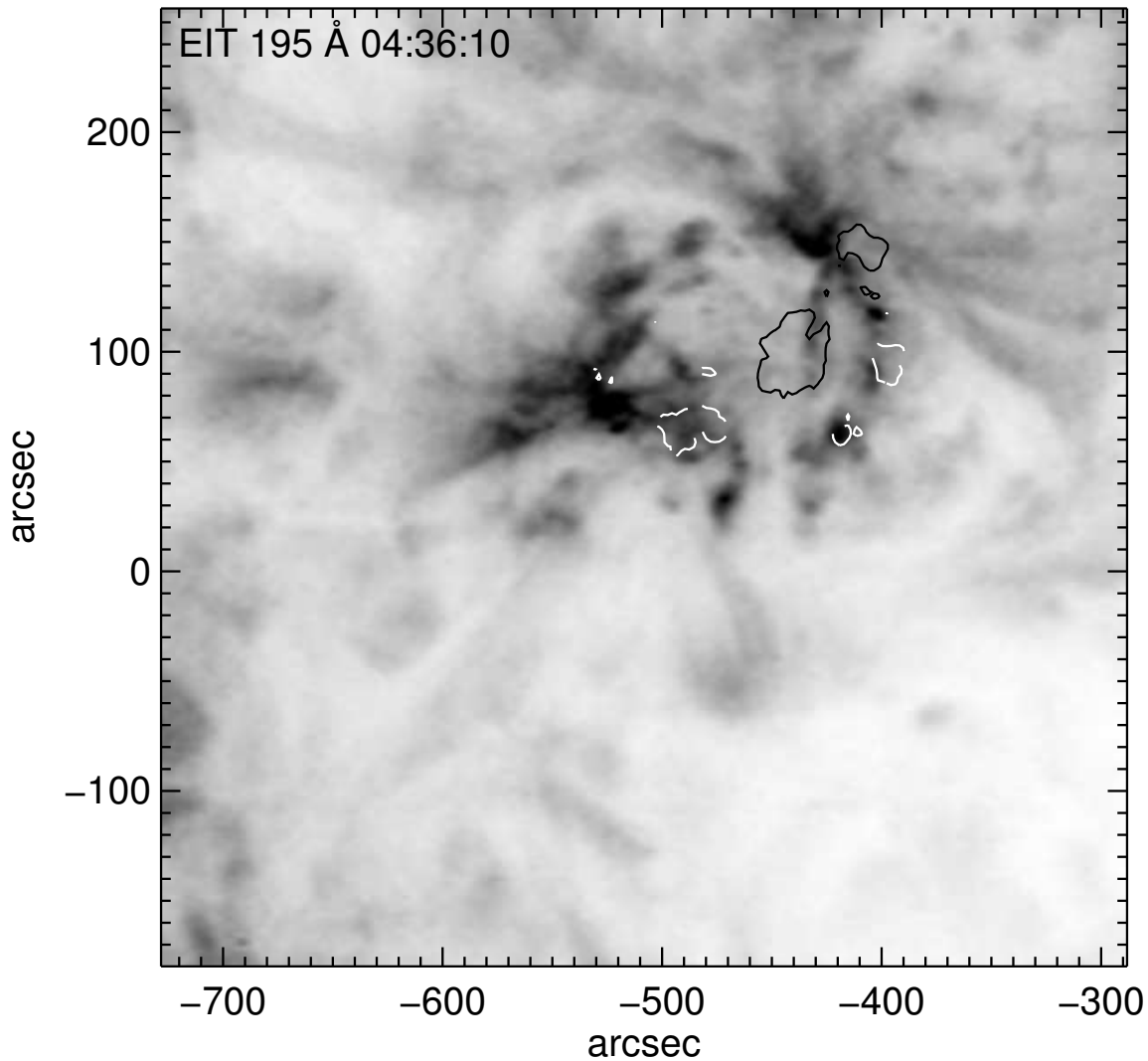


Figure 1. An EUV image (with reversed color table) of the active region in which the flare occurs. The image is from the Extreme-ultraviolet Imaging Telescope on the SOHO satellite in a passband dominated by the Fe XII 195 Å line. The contours show the longitudinal magnetic field data from the SOHO/MDI instrument ( $\pm 500$  Gauss).

subsequent EIT image at 05:12 UT: see Fig. 7 below). A gradual rise begins at 04:48 UT, changing to a rapid rise at 04:50 UT and a peak near 04:52 UT.

The radio data shown in Fig. 2 were obtained by the patrol telescopes of the US Air Force's Learmonth station. We show the flux at a frequency, 610 MHz, that is at the edge of GMRT's observing frequency band from 610 to 626 MHz, together with the patrol data at the adjacent frequencies of 410 and 1415 MHz and a representative microwave frequency of 8.8 GHz. The striking features of the 610 MHz burst are that it begins well before emission at other radio frequencies, the emission is quite bright (the burst peak is close to the total quiet-Sun flux of 58 sfu at this frequency, but yet the decimetric radio burst is barely if at all visible on the dynamic spectrum acquired by the Hiraio Radio Spectrograph), and there is no corresponding emission at 410 or 1415 MHz, implying that the decimetric burst is confined in frequency. The 610 MHz emission fluctuates rapidly. The emission at higher frequencies shows an impulsive spike close to 04:50 UT, followed by a more extended phase from 04:52 to 04:55 UT. The sharp rise in the impulsive spike appears to coincide with the change

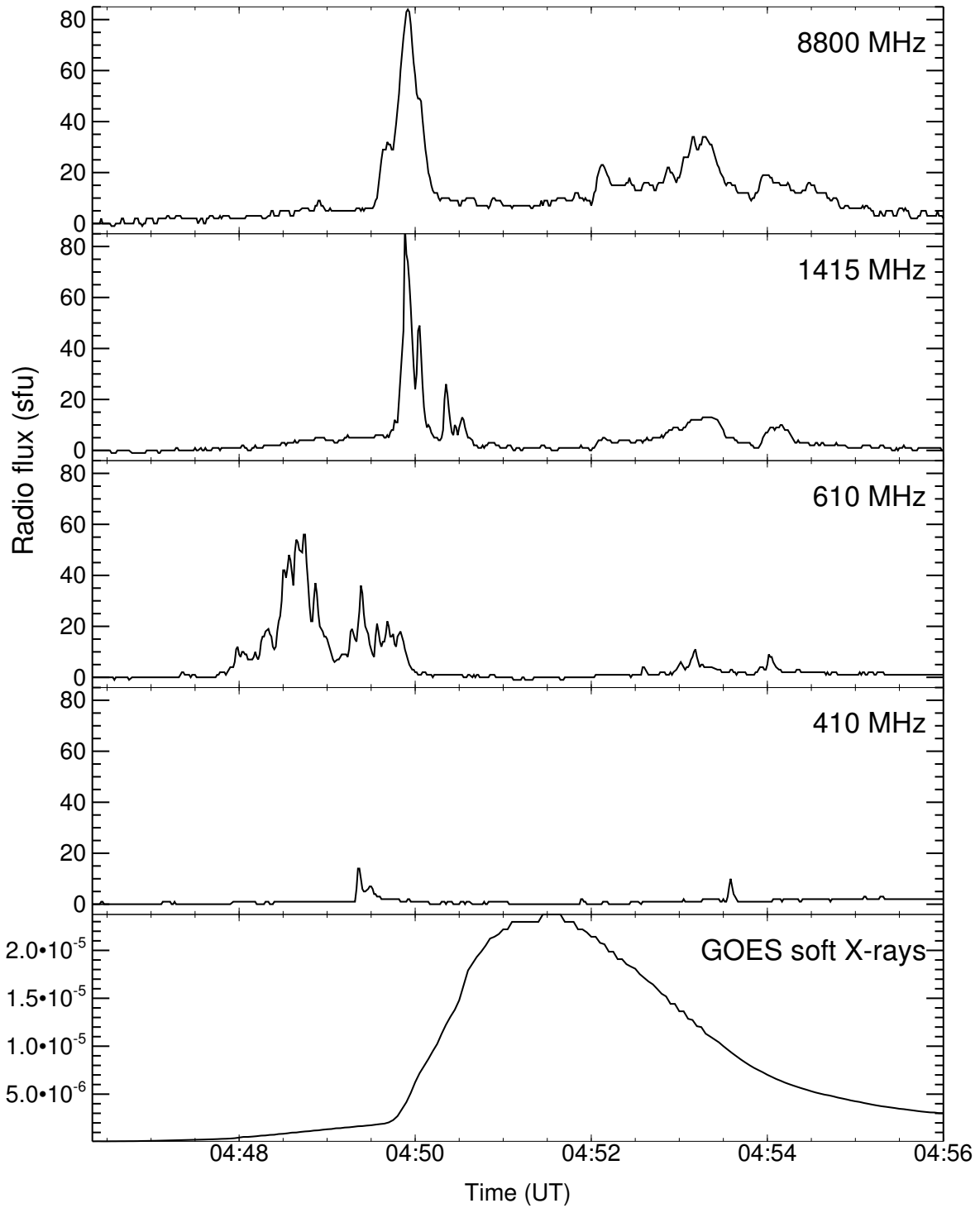


Figure 2. Lightcurves of the flare at selected radio frequencies (upper 4 panels, as labelled; units are solar flux units) and in soft X-rays (GOES 1–8 Å channel, lower panel; units are Watts  $m^{-2}$ ). The radio data are from the patrol telescopes at the Learmonth station of the Radio Solar Telescope Network operated by the US Air Force.

in slope of the soft X-ray emission, and the 610 MHz emission essentially terminates a few seconds later.

## 2.2. MICROWAVE IMAGING DATA

In the absence of RHESSI, TRACE or EIT images of the flare, 17 and 34 GHz images from the Nobeyama Radio Heliograph (NoRH) provide a valuable picture of the associated energetic phenomena in the lower atmosphere. Figure 3 shows a sample of radio images overlaid as contours on a white light image of the active region. The NoRH data were processed within the AIPS package using standard techniques at 1 s time resolution and deconvolved using restoring beams of  $12''$  at 17 GHz and  $10''$  at 34 GHz.

The image in the top left panel of Fig. 3 is a preflare image. Black contours show the 17 GHz emission, which is dominated by a gyroresonance source over the largest sunspot with a brightness temperature of 650000 K. A coronal magnetic field of order 2000 G (assuming third-harmonic opacity) is required to produce this source. The circular polarization image at 17 GHz shows this spot to be right circularly polarized, consistent with the expected extraordinary mode emission in the outward magnetic fields of the positively-polarized sunspot beneath it; the degree of polarization is 75%.

The remaining preflare emission at 17 GHz is weakly polarized if at all and we attribute it to thermal bremsstrahlung from coronal plasma. In particular, the peak in the 17 GHz emission at the trailing end of the active region, marked by a black cross, is at the location of the brightest emission in the EIT Fe XII image shown in Fig. 1. The preflare 34 GHz emission, which we expect to be completely dominated by thermal bremsstrahlung, also shows a peak at this location and local peaks at two other locations where the 17 GHz image also shows local peaks, consistent with the bremsstrahlung interpretation.

The flare emission is shown in the remaining five panels: in each case we have subtracted the preflare image before plotting for clarity. Throughout the event the radio emission is localized in two distinct sources, one essentially coincident with the gyroresonance source in the west and another  $60''$  away, adjacent to the preflare thermal peak in the trailing (eastern) part of the active region. During the early rise phase of the event, at 04:49:35, the western source over the large sunspot is the brighter source, and it shows clear double-structure along the north-east/south-west axis with the two components separated by about a beam width ( $12''$ ). For several seconds the main sunspot component location brightens without much change at the north-east location but then new component to the north-east, clearly seen in the 04:49:35 panel, is the stronger component for about 5 seconds. At this time the eastern source is barely visible. The western source dominates the flux during the impulsive spike at 04:50 UT at both 17 and 34 GHz, although the eastern source grows in relative importance during this period. By 04:52:03 UT, the western source has largely decayed away, particularly at 34 GHz, with the location shifting back towards the original location of the gyroresonance source, while the eastern source has continued to strengthen. During the extended phase from 04:52 to 04:55, the western source does not show much brightening at all, whereas the eastern source becomes even brighter than it was during the main impulsive spike. It too appears to be extended in the north-east/south-west direction during this time.

The two flare sources have opposite senses of circular polarization at 17 GHz: the western source is right-circularly-polarized (RCP), as was the associated preflare gyroresonance source, and the degree of polarization during the initial impulsive spike is of order 70%. The eastern source is left-circularly-polarized (LCP), at about 30% during the initial impulsive spike and then closer to 15% during the extended phase. NoRH light curves for the two distinct sources are shown in Figure 4. The curves are obtained by summing all the flux in disjoint boxes that contain the two sources. The figure confirms the impression given in the images of Fig. 3: the western source dominates the initial impulsive spike

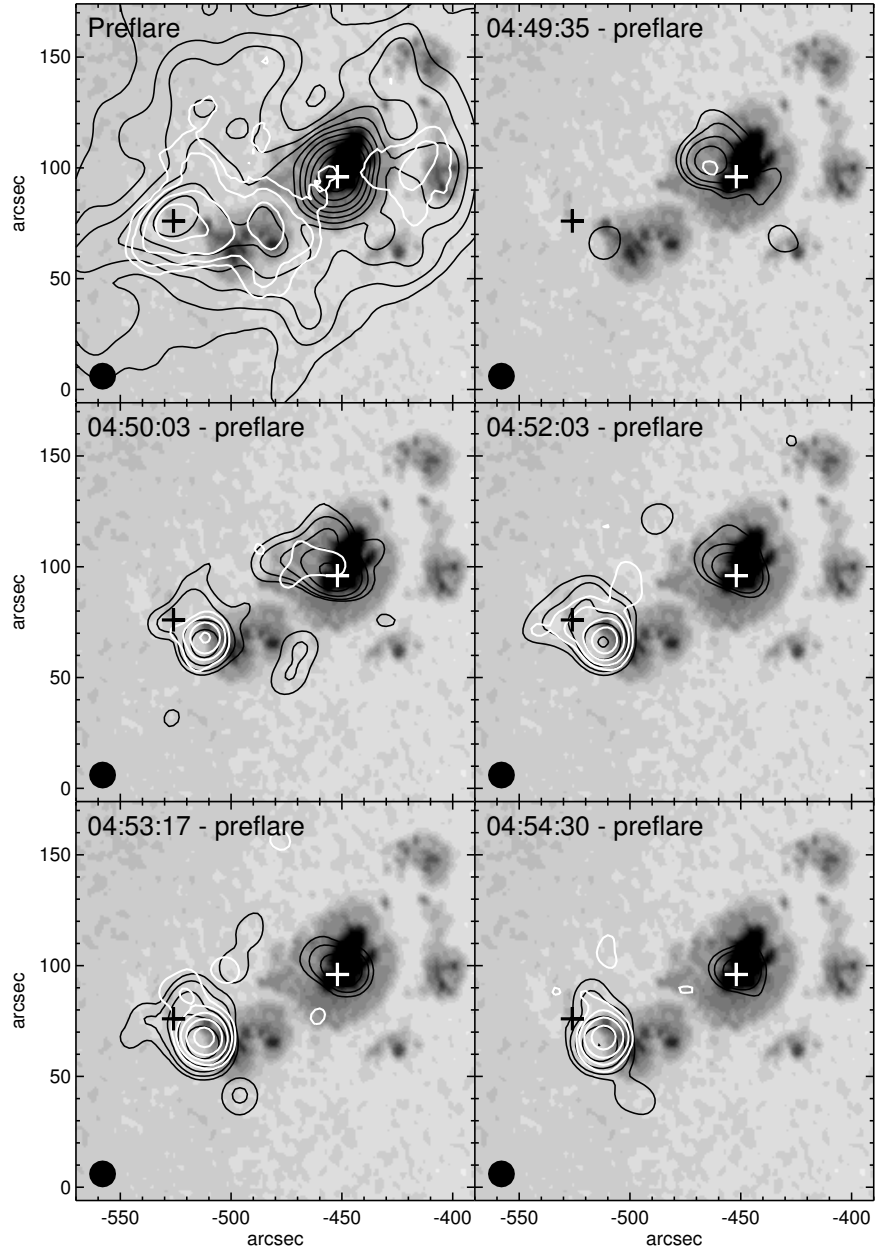


*Figure 3.* Images of the microwave radio emission from the flare at 17 GHz (black contours) and 34 GHz (white contours) from the Nobeyama Radio Heliograph, overlaid on a white-light image of the active region from the SOHO/MDI telescope. The image at top left shows preflare emission. The 17 GHz preflare image is dominated by a gyroresonance source over the leading sunspot in the active region; it is right circularly polarized, consistent with the positive polarity of the underlying spot, and has a brightness temperature of 650000 K. The lowest 17 GHz contour is at 5000 K and contours are logarithmically spaced, two contours being an increase by a factor  $e$ . The peak preflare brightness temperature at 34 GHz is 30000 K and 34 GHz preflare contours start at 5000 K. In subsequent panels the preflare images have been subtracted from the flare images before plotting, and the lowest contour is at 40000 K for 17 GHz and 20000 K for 34 GHz, except for 17 GHz at 04:50:03 when the bottom contour is 25000 K to emphasize the extension of the western source to the east. As reference points, the location of the preflare 17 GHz gyroresonance peak is marked by a white cross in all panels, and the location of the 17/34 GHz preflare peak at the eastern end of the active region is marked by a black cross. The resolution is  $12''$  at 17 GHz and  $10''$  at 34 GHz.

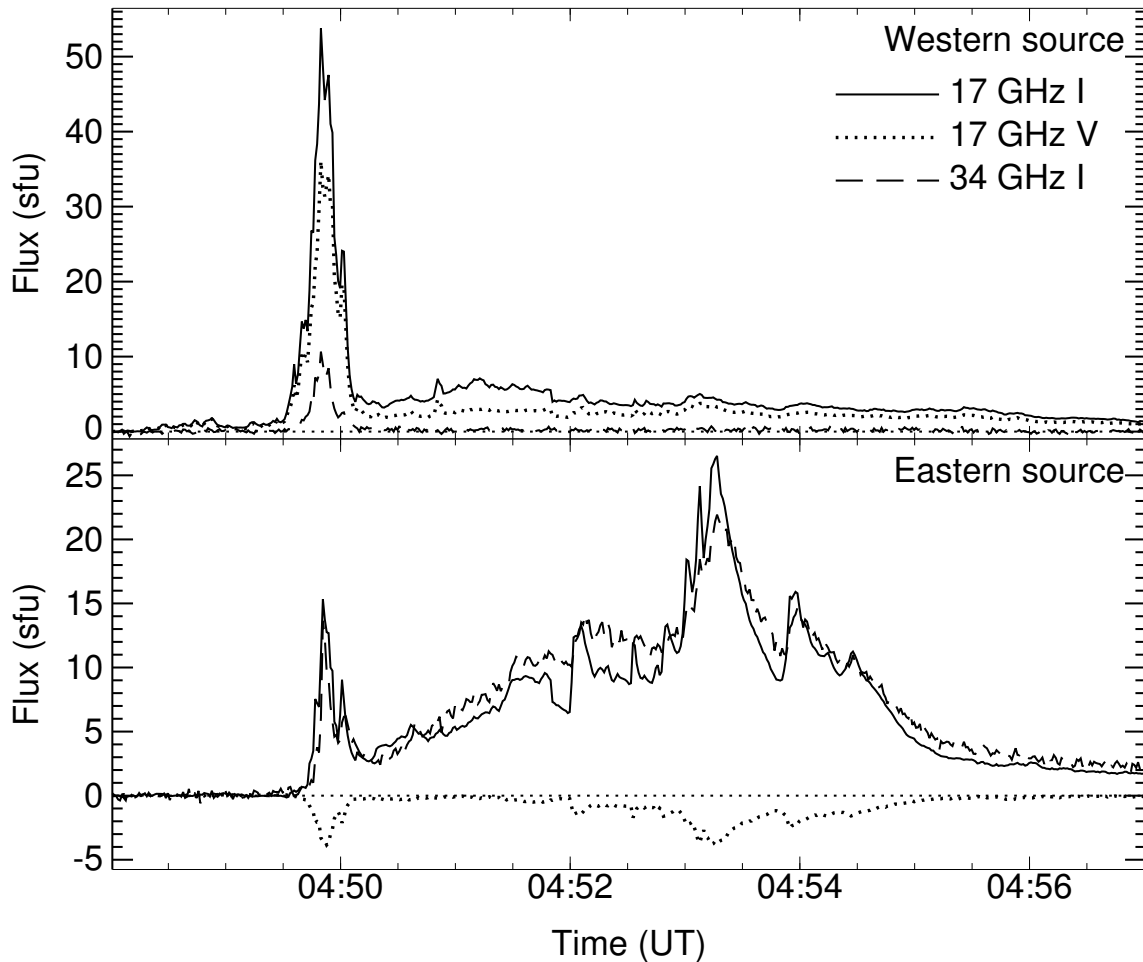


Figure 4. A comparison of the radio light curves for the eastern (lower panel) and western (upper panel) microwave flare sources. In each case the solid line is the 17 GHz total intensity, the dotted line is the 17 GHz circularly polarized intensity (Stokes V) and the dashed line is the 34 GHz total intensity. The time resolution is 1 second. The western source is positively circularly polarized and the eastern source is negatively polarized, both corresponding to  $x$  mode polarization with respect to the underlying photospheric magnetic field.

but is not bright during the subsequent extended phase when the eastern source provides nearly all of the emission. An interesting result that is not immediately apparent from the contour images is the difference in the spectra of the two sources: the western source has a typical nonthermal spectrum with the 17 GHz flux greatly exceeding the 34 GHz flux, whereas in the eastern source the 17 and 34 GHz fluxes are comparable. The spectrum of the eastern source is apparently flat from 17 to 34 GHz both in the initial spike and in the extended phase. Normally we would interpret this as a sign of optically thin thermal bremsstrahlung, but the spiky nature of the time profile and its lack of resemblance to the GOES soft X-ray light curve argue against such an interpretation and we believe it to be nonthermal emission with either an anomalously flat spectrum, or a peaked spectrum with the peak lying conveniently between 17 and 34 GHz.

The dominance of the radio emission by two oppositely-polarized compact sources suggests that they are footpoints at opposite ends of a loop system. We have looked for radio emission in the region between the two bright sources that might, e.g., indicate a magnetic connection between them, as has been seen in other events (e.g., Grechnev et al., 2003). There is no sign of such a connection during

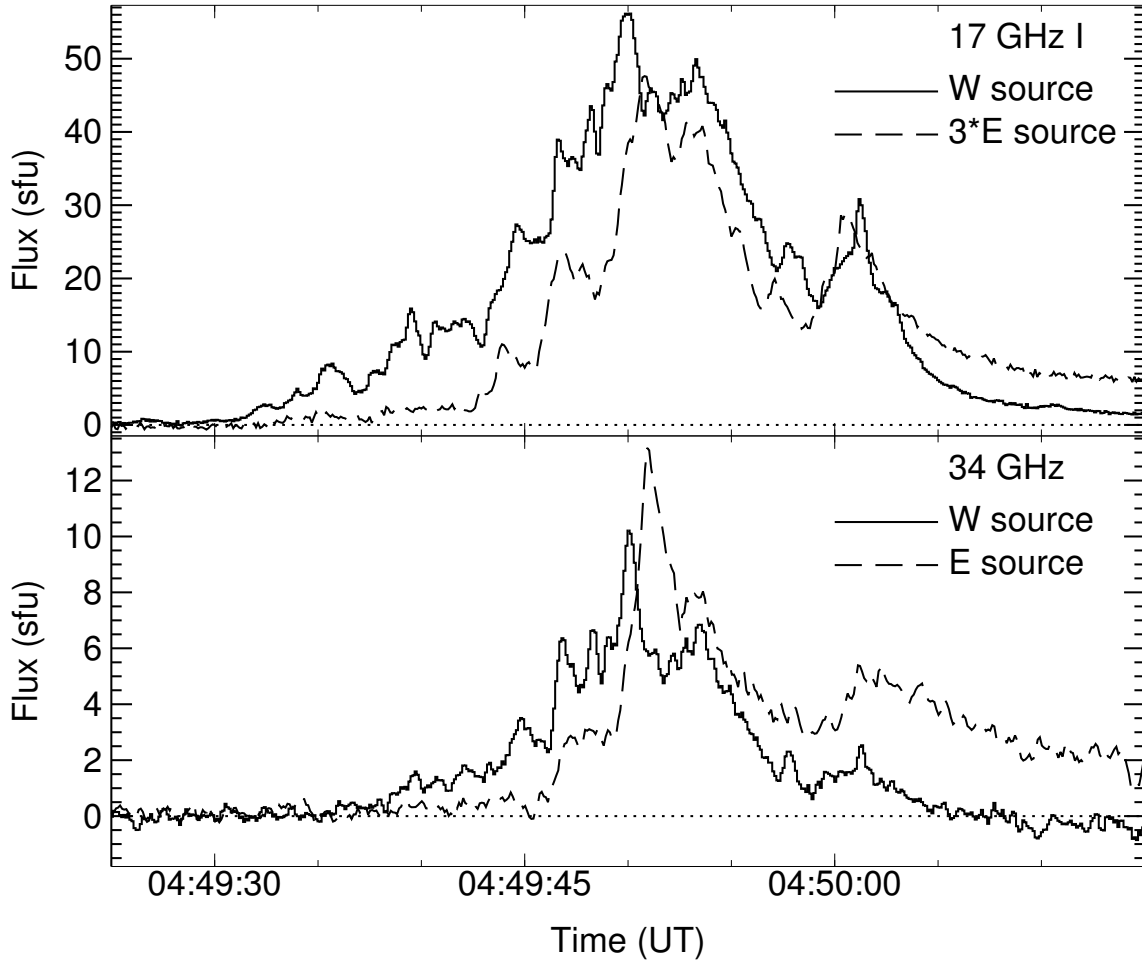


Figure 5. A comparison of the radio light curves for the eastern (dashed line) and western (solid histogram) microwave flare sources. In the upper panel the 17 GHz fluxes are compared, with the eastern source flux multiplied by 3 for comparison. In the lower panel the 34 GHz fluxes are plotted. The time resolution of the maps used to derive these fluxes is 0.1 s, but the 34 GHz fluxes have been subjected to a 3–point smoothing to reduce the noise level.

the rising phase of the impulsive spike, down to quite low levels of emission. The only period when such emission from a possible loop connection is visible in the radio images is from 04:49:45 to 04:50:10, when a finger of emission clearly extends eastwards from the western source towards the eastern source (see the panel at 04:50:03 in Fig. 3). After this time however the western source decays rapidly. There is no obvious feature at this loop position in the preflare image.

Another test for a magnetic connection between the two sources lies in similarity of the time profiles, on the assumption that the same nonthermal electrons propagate back and forth along magnetic field lines connecting the footpoints. We have already seen that both sources emit during the initial impulsive spike, but not during the extended phase. In other events it has been argued that a connection between two well-separated sources can exist early in the event but is disrupted during the impulsive phase and not apparent later in the event (Kundu et al., 2001). To investigate this further we plot in Figure 5 the light curves of the two sources during the initial impulsive spike using maps made with event data every 0.1 s. This comparison shows that the variations in the two sources appear to be well correlated from the peak onwards, but the emission begins in the western source well before it is seen in the eastern source, and the individual peaks are at slightly different times. No simple delay

improves the correlation of the light curves. At both 17 and 34 GHz, the time of peak flux in the eastern source is about  $1.0 \pm 0.2$  seconds later than the time of peak flux in the western source. For comparison, a 100 keV electron takes about 0.3 seconds to propagate from the western source to the eastern source, and the line of sight light–travel–time difference between the projected photospheric locations of the two sources ( $\sim 50''$ ) is about 0.1 seconds.

### 2.3. GMRT OBSERVATIONS AT 617 MHz

The GMRT is located about 80 km north of the city of Pune in Maharashtra, India. It consists of thirty 45m–diameter antennas spread over 25 km. Half of these are in a compact, randomly distributed array of about 1 km. The shortest baseline is 100m and the longest is 26 km. Further details about the GMRT can be found on the web page <http://www.gmrt.ncra.tifr.res.in>.

Solar observations with GMRT are described by Subramanian et al. (2003) and Kundu et al. (2004). For this observation a time resolution of 2.11 s was used. The data consist of 32 channels covering a 16 MHz bandwidth from 610 to 626 MHz. Data were calibrated using the source 3C283 (13 Jy) and converted to continuum visibilities with a nominal center frequency of 617.5 MHz. The outermost 11 antennas were not used for mapping since no flux was present on baselines with these antennas. Mapping was carried out with the remaining 16 good antennas, providing a beam size of order  $30''$ . At this frequency GMRT data do not contain sufficiently short baselines to image the solar disk, so the images are only sensitive to smaller structures. Solar attenuators are used for GMRT observations and their effect on the amplitudes is not well understood: nominally they are 30 dB attenuators. Fortunately, for this event we can compare the GMRT 617 MHz fluxes with the RSTN Learmonth 610 MHz fluxes. The two data sets show identical time structure, and we infer a scaling factor of order 2500 to correct the raw GMRT data to the RSTN flux levels. An additional calibration was applied to the burst data based on a self–calibration solution derived from data at the peak of the 617 MHz burst. The signal–to–noise achieved at the peak was almost 500, with the noise level in the images being of order  $3 \times 10^5$  K during low–flux periods. Both right and left circular polarizations are observed by GMRT. According to simple theory, emission close to the fundamental of the plasma frequency  $f_p = 9000\sqrt{n_e}$  due to conversion of electrostatic Langmuir waves, which is common at decimetric wavelengths, should be highly polarized in the sense of the ordinary mode because the extraordinary mode cannot propagate at frequencies below a cutoff at  $\approx f_p + f_B/2$ , where  $f_B = 2.8 \times 10^6 B_{\text{gauss}}$  is the electron gyrofrequency. On the other hand, plasma emission at a frequency  $2f_p$  due to coalescence of two Langmuir waves is generally weakly polarized for typical values of the coronal magnetic field strength in plasma emission sources (Zlotnik, 1981; Melrose et al., 1980).

GMRT images at selected times are shown in Figure 6. The top set of panels shows the pre–burst emission morphology in right (upper panels) and left (lower panels) circular polarizations. The RCP source has the appearance of a curved loop–shaped feature straddling the largest spot in the active region. However, the expected height of the 617 MHz emission combined with the eastern location of the active region produces considerable offsets due to projection of the 617 MHz emission onto the solar surface. The preflare RCP source is close to 100% circularly polarized, and hence is unlikely to be due to thermal emission. Such a high degree of polarization is consistent with plasma emission at the fundamental of  $f_p$ . The preflare source is actually quite stable through the entire event. The peak brightness temperature in this loop is  $2 \times 10^7$  K (an order of magnitude brighter than the peak in the preflare LCP images). If we assume, based on the high polarization, that it is fundamental plasma emission then the electron density in the source is  $5 \times 10^9 \text{ cm}^{-3}$ . This is an active region density and could arise in a low–lying loop, meaning there would be little shift due to projection. Note however that the EIT image (Fig. 1) does not show any loops corresponding to the 617 MHz RCP preflare

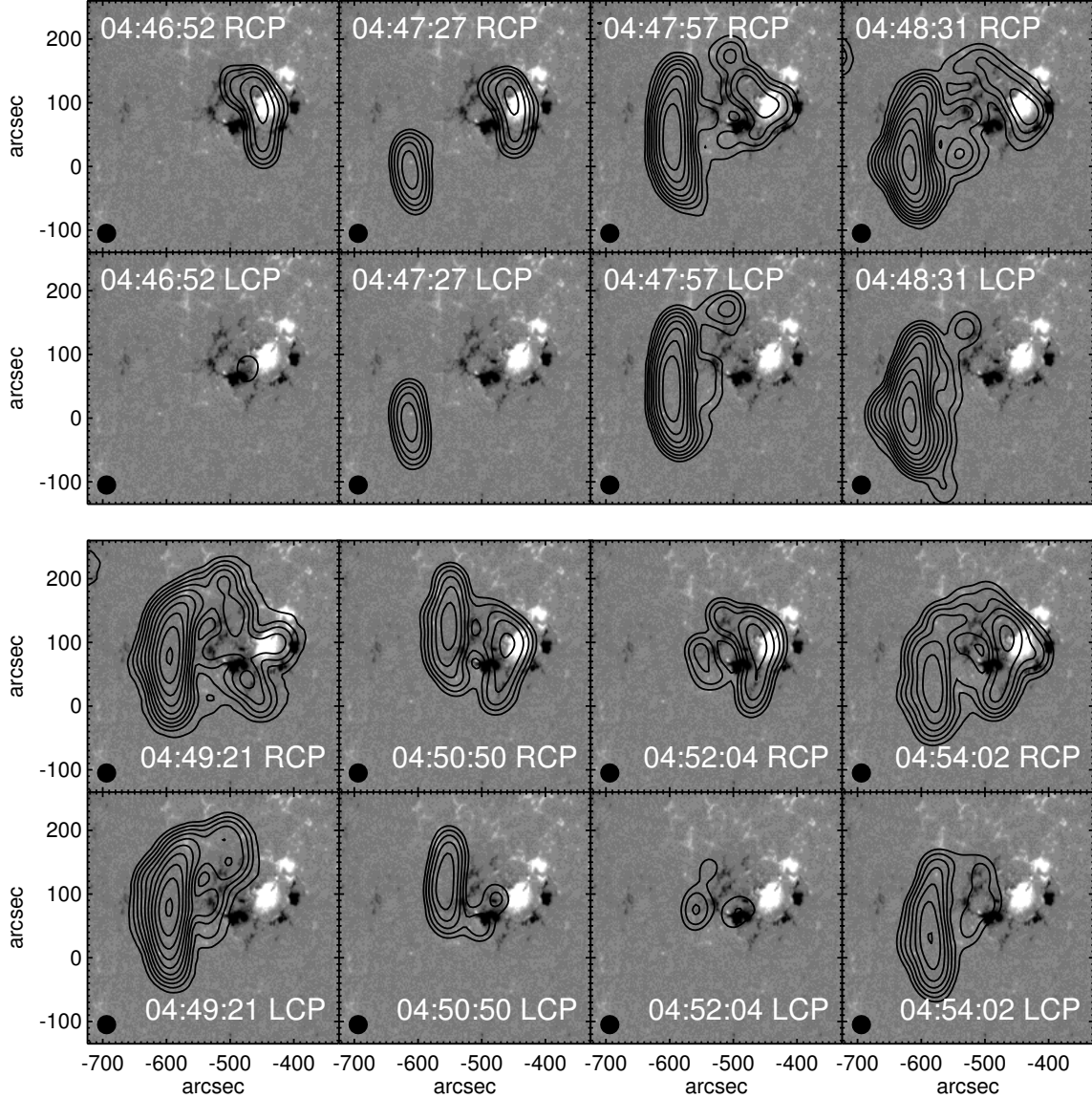


*Figure 6.* Contours of a sequence of 617 MHz GMRT images overlaid on an MDI magnetogram. The images are shown in pairs with the upper image displaying right circular polarization (RCP) and the lower image showing left circular polarization (LCP) at eight different times, as labelled, to demonstrate the different locations of the 617 MHz emission. The lowest 617 MHz contour is at  $1.5 \times 10^6$  K and contours are logarithmically spaced: every 4 contours is an order of magnitude increase in brightness temperature. The top row of figures corresponds to a pre-flare period. The loop-shaped feature visible in the RCP image over the active region has no counterpart in LCP, where the only steady feature is a much weaker compact source over the trailing negative polarity in the active region. The radio bursts all occur projected to the east of the active region in structures elongated north–south but with different locations at different times.

source. There is a very compact persistent source shown by the single contour in the 617 MHz LCP preflare image, but it is much weaker than the RCP source.

The light curve of the GMRT 617 MHz emission is compared directly with the NoRH microwave data in Figure 7. This figure also compares the morphology of the 617 MHz emission with the  $195 \text{ \AA}$  Fe XII EUV images from EIT. As noted earlier, the EIT coverage was unfortunate for this event, with the closest images being 12 minutes before and 24 minutes after the start of the 617 MHz emission.

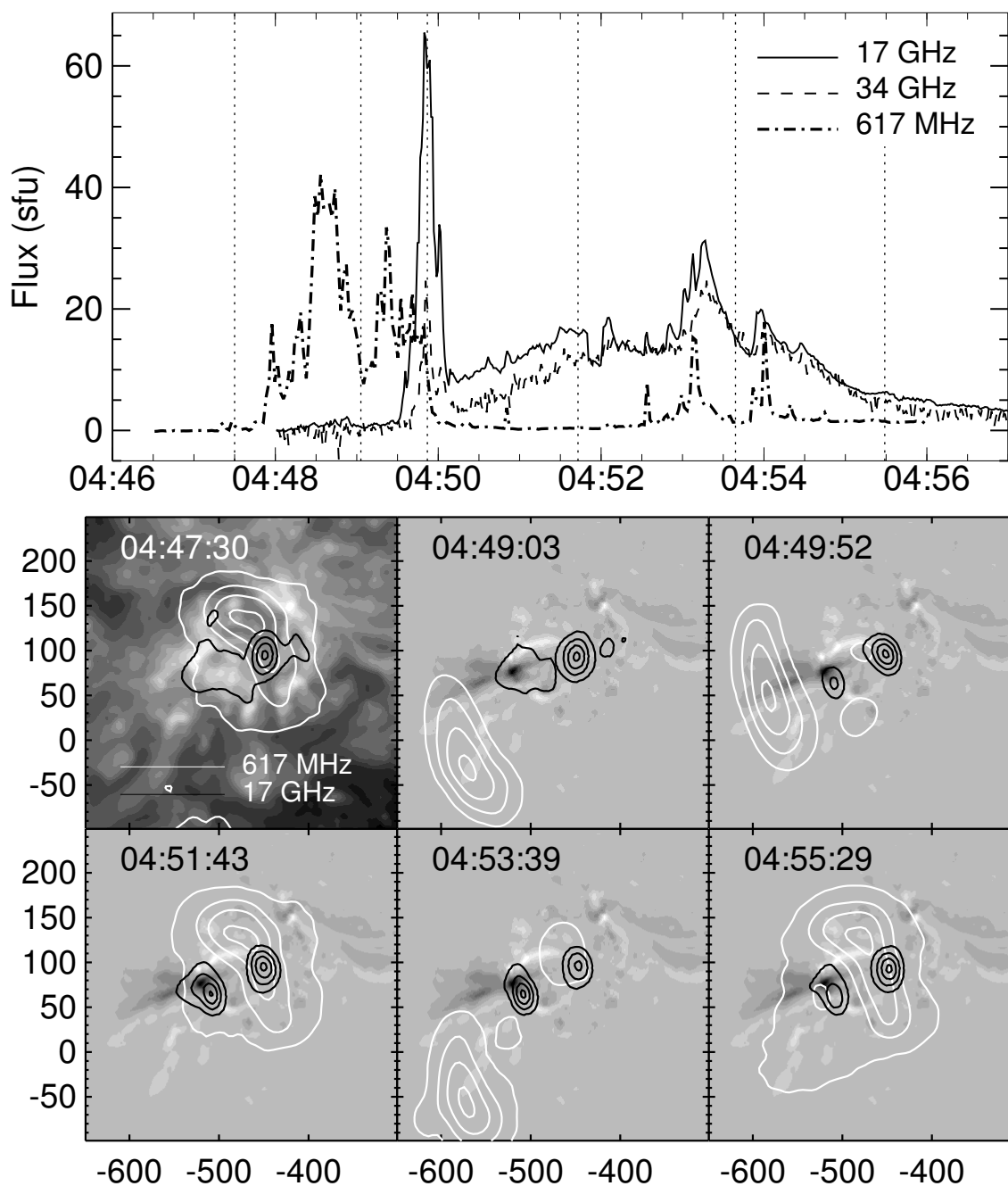


*Figure 7.* The upper panel shows a comparison of the radio light curves at 0.617 (dash-dot), 17 (solid) and 34 GHz (dashed line). The microwave fluxes are taken from the NoRH maps while the 0.617 GHz data are obtained from the GMRT maps. Note that the initial burst at 0.617 GHz precedes microwave activity and in fact dies away promptly on the onset of microwave emission. The vertical lines on the plot show the times of the images shown in the lower panels. In these panels contours of the 617 MHz RCP emission are shown in white and contours of 17 GHz emission are shown in black. Contour levels are at 5, 20, 50 and 90% of the maximum of each image plotted. The underlying greyscale images are EIT 195 Å images: in the first panel at 04:47:30 it is the actual postflare image at 05:12:42, while in subsequent panels it is the difference between the image at 05:12:42 and the preflare image at 04:36:10.

The EIT difference image does suggest the presence of a flare loop connecting the two 17 GHz flare sources. The 617 MHz radio burst effectively begins just before 04:48 UT (see the corresponding rows of panels in Fig. 6). Rapidly fluctuating emission continues for two minutes, followed by two minutes (04:50 – 04:52) with little activity at 617 MHz (the images look like the preflare images: e.g., see the panels for 04:52:04 in Fig. 6), and then there are additional bursts coinciding with peaks in the bright extended microwave phase from 04:52:30 to 04:54:45. In contrast to the preflare sources, all the 617 MHz flare emission is unpolarized (less than 5%, hence below the calibration uncertainty). Different burst peaks have quite different locations, but all arise projected to the south–east of the active region containing the flare, and despite their different locations, all the bursts show a similar morphology: they are elongated north–south and curved to resemble the tops of loops rooted in the active region and projected vertically above it. This common shape cannot be an artefact of the data processing since the preflare RCP source has quite a different shape that is preserved throughout the event; similarly, the varying location of the burst emission cannot be an artefact because the stable preflare RCP source is visible at its original location throughout the burst. Individual peaks within the 617 MHz burst with different locations seem to grow and decay in place as if they belong to separate energy releases on different magnetic field line bundles.

We noted earlier that there is no burst classification for the preflare 617 MHz emission because it does not show up on a dynamic spectrum. Benz et al. (2005) present statistics for decimetric radio bursts associated with flares and find that only two types of burst are commonly found in the preflare phase: Type III bursts and pulsations (see also Benz et al., 1983). They also note that the preflare Type III bursts typically do not extend down to lower meter–wavelength frequencies, i.e. they have a restricted frequency range, as is true both of typical decimetric pulsations and of this event. Thus the preflare emission seen here could in principle be either Type III bursts or pulsations.

Inspection of the visibilities confirms that the burst sources are well resolved at the  $30''$  resolution of the data. The image at 04:48:31 corresponds to the peak brightness and size for the 617 MHz emission: the peak brightness temperature is just over  $4 \times 10^8$  K and the length is approximately  $200''$  or 140000 km. If we assume second–harmonic plasma emission, consistent with the low polarization, then the electron density in the radio source is  $1 \times 10^9$  cm $^{-3}$ . Note that there is no sign of corresponding loops in the EIT images of the region (Fig. 1), and no obvious magnetic features in the magnetogram to the south–east of the active region that should be connected to it by such loops, arguing that the loops illuminated by the GMRT emission are indeed tall loops with both footpoints anchored close to the active region that appear located to the south–east due to projection effects. The inferred height of the loop illuminated at 04:48:31 if it lies vertically above the active region at  $30^\circ$  east, appearing about  $180''$  east of the active region, is 250000 km. The density of  $10^9$  cm $^{-3}$  is rather large for such a height: in the density model of Aschwanden and Benz (1995) (based on Type III bursts), this density occurs at a height of order 40000 km.

### 3. Discussion

The goal of this paper is to determine the morphology of emission at decimetric wavelengths during a solar flare, and to use that morphology to place constraints on the coronal magnetic field topology during the event. This event is not typical of decimetric emission from a solar flare in that, while it is not uncommon for decimetric emission to occur prior to the impulsive phase of flares (Benz et al., 2005), it is not usual for the decimetric emission to peak well before the impulsive phase starts. Notwithstanding this feature, the observations reveal a remarkable pattern.

The decimetric images at 617 MHz from GMRT show an interesting distinctive morphology: sources are seen in projection some 120000 km from the flaring active region, consistent with a height

of order 250000 km above the solar surface if they are loops rooted in and radially extended above the active region. The sources appear highly elongated north–south and are curved in the direction expected if they are located at the tops of loops radially extended above the active region, but with footpoints along a north–south axis rather than the east–west axis suggested by the distribution of magnetic polarity in the active region at the photosphere. However, while maintaining this morphology, the source locations are distinctly different during different peaks within the 617 MHz light curve, as if different loops were connected to the acceleration site at different times. No strong Type III bursts are evident in the dynamic spectrum of this event, and the lack of emission at lower frequencies, such as we would expect to see from electron beams on open field lines, may be consistent with an origin on closed field lines as this interpretation suggests, possibly pulsations as discussed earlier.

The ability to discern source shifts as small as a few tens of arcseconds between adjacent decimetric burst peaks relies on the excellent spatial resolution of the GMRT data. Subarcminute resolution at similar frequencies has been possible with the VLA in extended configurations at 330 MHz (corresponding to a plasma density 4 times smaller than at 617 MHz if plasma emission is the responsible emission mechanism as generally assumed), and at the much higher frequency of 1.4 GHz (corresponding to 5 times larger density). The Nançay Radio Heliograph can achieve a resolution of order  $1'$  at 410 and 432 MHz (e.g., Vilmer et al., 2002, Pick et al., 2005) and has seen source shifts within flare radio emission, but they tend to be on much larger scales (e.g., Maia et al., 2001). Most of the observations at decimetric frequencies show very large burst sources, at least partly due to scattering in the solar atmosphere (Bastian, 1994); frequently, a pre-existing noise storm source is seen to be leading (west of) the photospheric active region and a large (typically  $2'$  or more) flare source appears trailing the active region (e.g., Willson, 2002, Willson, 2005), as is the case in this event. Willson et al. (1998b) observed an arch-shaped source just above the limb at 75 MHz using the VLA, but it was not associated with a flare, and it lasted for several hours. Arc-like sources have been seen in noise storms at 330 MHz (e.g., Willson et al., 1997), but they too are long-lasting sources that are not clearly flare-associated. Some highly elongated sources have been seen at or above the limb, with the long dimension of the radio source frequently oriented approximately parallel to the limb (Willson et al., 1990; Willson et al., 1992; Willson et al., 1998a).

The apparent location of the radio burst sources in this event at the top of closed magnetic field lines, indicated by the shapes of the sources, also suggests that the radiating electrons are confined to the loop tops. A natural explanation for this observation would be that the electrons have large pitch angles and reside on magnetic field lines with a gradient in field strength from loop top to footpoints, so that magnetic mirroring traps the electrons near the loop tops. Such electrons would have a “pancake” pitch angle distribution, peaked at  $90^\circ$ , similar to those commonly seen near the geomagnetic equator in the Earth’s radiation belts (e.g., Meredith et al., 1999, Horne and Thorne, 2000). Such pitch angle distributions can arise either by the loss of all particles at smaller pitch angles, as occurs via precipitation into the solar chromosphere in solar flares, or by an instability that drives electrons to larger pitch angles. In this event we see no sign of electrons at lower pitch angles that would be expected to produce X-rays and microwave emission as they precipitate. A velocity distribution concentrated at pitch angles near  $90^\circ$  does not by itself guarantee coherent emission: the electron cyclotron maser instability only operates if there is also a region of positive gradient in the magnitude of velocity, and similarly Langmuir waves are only likely to be generated under the same conditions (a “gap” velocity distribution with a large loss cone: see Hewitt and Melrose, 1985 and Wentzel, 1985). The low polarization of the 617 MHz burst emission is also a strong constraint on the emission mechanism: a gap velocity distribution with a large loss cone can produce weakly polarized second-harmonic plasma emission (Hewitt and Melrose, 1985), but fundamental plasma emission can also be weakly polarized if depolarization takes place during propagation out of the corona, e.g., due

to scattering off low-frequency waves (Wentzel et al., 1986) or reflection off sharp density boundaries (Melrose, 2005).

The microwave data from NoRH reveal activity lower in the solar corona and show emission spread over a surface dimension of order 50000 km, with a complex spatial pattern: activity begins in a western source that becomes a double source early in the event and remains spatially extended, but later in the event an eastern source, also spatially extended, comes to dominate. There is evidence for a connection between the two sources only during a brief period in the decay of the western source at the end of the initial impulsive spike. The light curves of the eastern and western sources appear quite similar during this initial impulsive spike, but the times of the individual peaks in the light curve do not match and no simple delay between them improves their correlation, so we cannot infer that a single accelerator supplies electrons to both sources even during this period. At other times during the event the light curves of the eastern and western sources are very different, implying that their activity is not directly related.

The main activity at 617 MHz precedes that at microwave frequencies by about 2 minutes: i.e., there is evidence that energy release is taking place at heights of order  $10^5$  km for 2 minutes before any evidence is seen in the lower corona. This suggests a model in which the solar flare activity in the low corona is a response to magnetic restructuring much higher in the corona. Such a model is suggestive of eruptive flare theories such as the breakout model (Antiochos et al., 1999; Aulanier et al., 2000; Sterling and Moore, 2001) for filament eruptions, in which the filament lies over a neutral line and is held down by closed magnetic field lines that loop over the top of the filament. Reconnection between the overlying closed field lines and the magnetic field of an adjacent flux system gradually erode away the tethering field lines until enough of the restraining flux is eaten away for the filament to erupt under its buoyancy, or under the driving force provided by, e.g., emerging flux. Thus in the breakout model activity starts higher in the corona where the restraining field lines adjoin a neighbouring flux system. However, no coronal mass ejection was detected in conjunction with this flare, so the restructuring in this case did not lead to an eruption. In other models such as the tether-cutting model (Sturrock, 1989; Moore et al., 1997; Moore et al., 2001), activity starts low down and then moves upwards with the filament: the filament lies in a region of strongly sheared fields, and once the shear exceeds a certain value the filament has to erupt to relieve the shear stress, forcing its way out through the overlaying fields, disrupting them as it goes. The “CSHKP” model (Carmichael, 1964; Sturrock, 1968; Hirayama, 1974; Kopp and Pneuman, 1976) is also an eruptive model in which reconnection occurs at a considerable height in a Y-type neutral current sheet, and energy then propagates downwards in the form of energetic particles, but in this model we expect an obvious flare loop system formed by the reconnection to be evident and no such loops are seen in this event; further, reconnecting open field lines are intrinsic to this model, whereas this event was apparently dominated by closed field lines. This is the characteristic of confined flares described by Moore et al. (2001), where the flare is started by reconnection low in the sheared core field, but the resulting expansion of the core field is halted within the domain of the overlying bipole field. However this model cannot apply to our event since activity starts high in the corona, not low down.

#### 4. Summary and Conclusions

GMRT observations of a confined solar flare at 617 MHz show a remarkable morphology for two minutes preceding the impulsive phase of the flare. Microwave images at 17 and 34 GHz show flare emission with the not uncommon pattern of two oppositely circularly-polarized sources at opposite ends of an active region, 40000 km apart. The two sources have differing radio spectra, and light curves that are similar in the initial impulsive spike but differ as the flare evolves.

However, the GMRT images reveal a very different morphology: they appear to show a succession of high loops lighting up, apparently in arc-shaped features close to the tops of the loops. The loops lie radially above the active region in which the impulsive phase of the flare subsequently occurs, at a height of order 250000 km. They seem to connect the active region to a location of very weak field about 200000 km away, which shows no signs of activity at other wavelengths. The decimetric emission is very bursty, and discrete bursts appear with the same morphology but projected onto different spatial locations, as if energy releases occur sequentially on different bundles of field lines. The morphology suggests, but does not prove, emission from electrons with a “pancake” velocity distribution, i.e., electrons with pitch angles near  $90^\circ$  confined to the tops of magnetic loops.

In this flare, the fact that the 617 MHz activity at high altitudes precedes the impulsive phase of the flare indicates a mechanism in which the restructuring in the high corona leads to the flare occurring in the lower corona. This feature in conjunction with the fact that the flare appears to be confined to closed field lines is not consistent with most flare models.

### Acknowledgements

Solar research at the University of Maryland is supported by NSF grant ATM 02-33907 and NASA grants NAG 5-10175, NAG 5-12860, NAG 5-12732 and NAG 5-11872. We thank the staff of the GMRT who have made these observations possible. GMRT is run by the National Centre for Radio Astrophysics of the Tata Institute of Fundamental Research. We thank the referee for valuable suggestions.

### References

- Antiochos, S. K., C. R. Devore, and J. A. Klimchuk: 1999. *Astrophys. J.* **510**, 485–493.
- Aschwanden, M. J. and A. O. Benz: 1995. *Astrophys. J.* **438**, 997–1012.
- Aulanier, G., E. E. DeLuca, S. K. Antiochos, R. A. McMullen, and L. Golub: 2000. *Astrophys. J.* **540**, 1126–1142.
- Bastian, T.: 1994. *Astrophys. J.* **426**, 774.
- Benz, A. O.: 2004. In: D. E. Gary and C. U. Keller (eds.): *Solar and Space Weather Radiophysics*. Dordrecht, pp. 203–221.
- Benz, A. O., C. H. Barrow, B. R. Dennis, M. Pick, A. Raoult, and G. Simnett: 1983. *Solar Phys.* **83**, 267–283.
- Benz, A. O., P. C. Grigis, A. Csillaghy, and P. Saint-Hilaire: 2005. *Solar Phys.* **226**, 121–142.
- Carmichael, H.: 1964. In: W. N. Hess (ed.): *AAS-NASA Symposium on Solar Flares*. p. 451.
- Dulk, G. A. and R. M. Winglee: 1987. *Solar Phys.* **113**, 187–192.
- Gray, A., M. I. Large, D. Campbell-Wilson, and L. Cram: 1990. *Solar Phys.* **125**, 359.
- Grechnev, V. V., S. M. White, and M. R. Kundu: 2003. *Astrophys. J.* **588**, 1163–1175.
- Güdel, M. and A. O. Benz: 1988. *Astron. Astrophys. Supp. Ser.* **75**, 243.
- Hewitt, R. G. and D. B. Melrose: 1985. *Solar Phys.* **96**, 157.
- Hirayama, T.: 1974. *Solar Phys.* **34**, 323.
- Horne, R. B. and R. M. Thorne: 2000. *J. Geophys. Res.* **105**, 5391–5402.
- Islaker, H. and A. O. Benz: 1994. *Astron. Astrophys. Supp. Ser.* **104**, 145–160.
- Jiříčka, K., M. Karlický, and H. Mészárosová: 2002. In: *ESA SP-477: Solspa 2001, Proceedings of the Second Solar Cycle and Space Weather Euroconference*. pp. 351–354.
- Jiříčka, K., M. Karlický, H. Mészárosová, and V. Snížek: 2001. *Astron. Astrophys.* **375**, 243–250.
- Kopp, R. A. and G. W. Pneuman: 1976. *Solar Phys.* **50**, 85.
- Kundu, M. R., V. V. Grechnev, V. I. Garaimov, and S. M. White: 2001. *Astrophys. J.* **563**, 389.
- Kundu, M. R., S. M. White, V. I. Garaimov, P. K. Manoharan, P. Subramanian, S. Ananthakrishnan, and P. Janardhan: 2004. *Astrophys. J.* **607**, 530.
- Maia, D., M. Pick, S. E. I. Hawkins, and S. Krucker: 2001. *Astrophys. J.* **560**, 1058–1064.
- Melrose, D. B.: 1999. *Astrophys. Space Sci.* **264**, 401–410.
- Melrose, D. B.: 2005. *Astrophys. J.* submitted.

- Melrose, D. B., G. A. Dulk, and D. E. Gary: 1980. *Proc. Astron. Soc. Aust.* **4**, 50–53.
- Mercier, C., P. Subramanian, A. Kerdraon, M. Pick, , S. Ananthakrishnan, and P. Janardhan: 2005. *Astron. Astrophys.* submitted.
- Meredith, N. P., A. D. Johnstone, S. Szita, R. B. Horne, and R. R. Anderson: 1999. *J. Geophys. Res.* **104**, 12431–12444.
- Moore, R. L., B. Schmieder, D. H. Hathaway, and T. D. Tarbell: 1997. *Solar Phys.* **176**, 153–169.
- Moore, R. L., A. C. Sterling, H. S. Hudson, and J. R. Lemen: 2001. *Astrophys. J.* **552**, 833–848.
- Pick, M., J.-M. Malherbe, A. Kerdraon, and D. J. F. Maia: 2005. *Astrophys. J. (Lett.)* **631**, L97–L100.
- Sterling, A. C. and R. L. Moore: 2001. *J. Geophys. Res.* **106**, 25227–25238.
- Sturrock, P. A.: 1968. In: *IAU Symp. 35: Structure and Development of Solar Active Regions*, Vol. 35. p. 471.
- Sturrock, P. A.: 1989. *Solar Phys.* **121**, 387–397.
- Subramanian, P., S. Ananthakrishnan, P. Janardhan, M. R. Kundu, S. M. White, and V. I. Garaimov: 2003. *Solar Phys.* **218**, 247.
- Vilmer, N., S. Krucker, R. P. Lin, and The Rhesi Team: 2002. *Solar Phys.* **210**, 261–272.
- Wentzel, D. G.: 1985. *Astrophys. J.* **296**, 278.
- Wentzel, D. G., P. Zlobec, and M. Messerotti: 1986. *Astron. Astrophys.* **159**, 40–48.
- Willson, R. F.: 2002. *Solar Phys.* **211**, 289–313.
- Willson, R. F.: 2005. *Advances in Space Research* **35**, 1813–1821.
- Willson, R. F., M. J. Aschwanden, and A. O. Benz: 1992. In: *The Compton Observatory Science Workshop*. pp. 515–521.
- Willson, R. F., J. N. Kile, and B. Rothberg: 1997. *Solar Phys.* **170**, 299–320.
- Willson, R. F., K. R. Lang, and M. Liggett: 1990. *Astrophys. J.* **350**, 856–867.
- Willson, R. F., K. R. Lang, B. Thompson, U. Schuehle, and D. M. Zarro: 1998a. In: *ASP Conf. Ser. 154: Cool Stars, Stellar Systems, and the Sun*. p. 727.
- Willson, R. F., S. L. Redfield, K. R. Lang, B. J. Thompson, and O. C. St. Cyr: 1998b. *Astrophys. J. (Lett.)* **504**, L117.
- Zlotnik, E. I.: 1981. *Astron. Astrophys.* **101**, 250–258.